An experimental study with renewable fuels using ECN Spray A and D nozzles.

Authors:

José V. Pastor, José M. García-Oliver, Carlos Micó, Alba A. García-Carrero

CMT - Motores Térmicos /Universitat Politècnica de València

Abstract

The decarbonization process of the automotive industry and the road transport sector has raised the interest on the development of cleaner fuels. A proper characterization of their properties and behavior under different operating conditions is mandatory to achieve an effective implementation in commercial engines. With this objective, the current work presents a comparison of two injectors from the Engine Combustion Network (ECN), namely Spray A and Spray D injectors, in terms of spray characteristics and combustion behavior for different fuels: diesel, dodecane, Hydrotreated Vegetable Oil (HVO) and two types of oxymethylene ethers (OME_1 and OME_x). The aim is to analyze how differences in nozzle geometry affect the behavior of different types of fuels. The experiments were carried out in a High Temperature and High Pressure test rig and operating conditions were chosen following ECN guidelines. Visualization techniques such as high speed schlieren imaging, OH^* chemiluminescence and diffused back illumination were implemented to analyze the differences in liquid length, vapor penetration, auto ignition, flame lift-off length and soot formation for both nozzles. In general, results showed the same trend for all the fuels tested: longer liquid length and faster vapor penetration for Spray D, as well as higher ignition delay and longer lift-off length. However, it was found that these parameters were less sensitive to the nozzle diameter for the oxygenated fuels tested. Furthermore, a different trend was observed for OME_1, in terms of ignition behavior, in comparison to the other fuels. In terms of soot production, the Spray D nozzle increases its formation with the non-oxygenated fuels. In contrast, no soot was observed with the oxygenated ones under any operating conditions.

1 Introduction

Restrictions related to pollutant emissions such as Particle Matter (PM) and NO_x, in combination with the new regulation of CO_2 emissions, drive the interest in advanced combustion modes including the use of alternative fuels as a path to achieve these requirements. The goal to achieve “zero impact emission vehicles” is very close [1]

Fuel properties determine the emission characteristics. For example, the pathway to form soot is determined by the appearance of Polycyclic Aromatic Hydrocarbons (PAHs), which is directly linked with the molecular structure of the fuel. In fact, it is known that an increase of the C/H ratio in the fuel molecule produces an increase in soot concentration [2]. Although a reduction on pollutant emissions

can be achieved by means of after-treatment systems, its combination with in-cylinder pollutants reduction strategies will be critical for the future of the internal combustion engine (ICE). It is known that the engine combustion is complex, requiring substantial effort to understand the effect of variables such as the fuel features. In this context, the search for alternative fuels to replace the conventional ones has been one of the targets of many research works during the last decade.

New fuels obtained from renewable sources are of great interest because they can also contribute to the reduction of ICE carbon footprint. A closed cycle can be built where CO_2 emitted during combustion is used to produce more fuel. Processes such as dehydration, oligomerization and hydrogenation can be implemented to obtain alcohols, ethers and different oils from renewable sources. One of most promising proposals on this regard is the Hydrotreated Vegetal Oil (HVO). It can be obtained from hydrogenation of vegetal oils, resulting in a paraffinic structure without oxygen on its composition and with a similar chain length to diesel. It has shown potential to reduce PM, NO_x and CO_2 at the same time [3]

Fuels with high oxygen content in their molecular structure, such as oxymethylene ethers have shown very interesting results, too. They can be produced by a synthetic process that consumes CO_2 and water [4,5]. Those fuels have different composition and structure than conventional fuels used as diesel surrogates. Therefore, characterizing their behavior and performance in the combustion process can contribute to the development of better combustion models and strategies. Experimental studies carried out with oxymethylene ethers have shown low NO_x and soot emissions levels [6,7].

In the same way that studying the combustion performance of any fuel in an ICE is important, it is also important to describe how the behavior in terms of atomization and spray development is. Both processes are strongly influenced by the physical processes occurring inside the cylinder [8], which at the same time depend on nozzle characteristics and injection-related operating conditions. Parameters such as injection pressure, needle lift, orifice conicity or orifice geometry control flow dynamics and behavior at the outlet of the nozzle [9–11]. The nozzle geometry affects the atomization process and, therefore, the size of fuel droplets. Consequently, fuel vaporization as well as the fuel-air mixing are also affected. This has a strong impact on combustion development and soot formation [12].

Considering all the above mentioned, the current work proposes a detailed study of the influence of different nozzle geometries on the spray evolution and combustion behavior of different renewable fuels. The main objective is to determine how the nozzle affects the behavior of fuels with different properties. For this purpose, two nozzles from the Engine Combustion Network (ECN) [13] namely Spray A and Spray D were used with five different fuels: conventional diesel, dodecane, Hydrotreated Vegetable Oil (HVO) and two oxymethylene ethers (OME_1 and OME_x).

The study was carried out in a High Pressure and High Temperature rig (HPHT), under similar operating conditions as those defined as “standard” by the ECN [13]. High-speed schlieren and OH^* chemiluminescence were implemented to measure some characteristic parameters such as spray vapor

penetration, ignition delay and lift-off length. Besides, Diffused Back Illumination (DBI) was applied to measure the liquid length and characterize the soot production of all the fuels with both nozzles. The results presented in this work will provide more insight on the influence of different nozzle geometries on the combustion behavior of fuels with different properties such as those proposed here. Besides, the data presented here will improve the database of the ECN regarding the fuels considered and the two nozzle geometries. All in all, these results will contribute to the development and implementation of alternative fuels as well as on the improvement of combustion models.

2 Experimental setup

2.1 High Pressure and High Temperature Rig

The experiments were carried out in a High Pressure and High Temperature facility (HPHT). This rig allows to simulate the thermodynamic conditions found inside the cylinder of a compression ignition engine when the fuel is injected. Besides, it provides a wide optical access to the combustion chamber, for the application of wide variety of visualization techniques. Parameters such as ambient gas composition, pressure and temperature can be controlled independently to obtain between 0 and 21% of oxygen concentration, temperatures up to 1100 K and pressures up to 15 MPa. Moreover, in this vessel it is possible to obtain a homogeneous temperature field in the region of interest, which reduces the uncertainties that could be associated to engine transients. The thermodynamic conditions are steady during long time periods therefore it is possible to get reliable statistical results. The injection event takes place every 4 seconds. With this frequency it is ensured that the combustion residuals are scavenged and the steady thermodynamic conditions are achieved for each combustion event. A wider and detailed description about the facility and boundary conditions can be found in [14].

2.2 Nozzles and fuel characteristics

In this study two single-hole injectors with different nozzle geometry from the Engine Combustion Network (ECN) were used, namely Spray A and Spray D [13]. No cavitation problems have been observed in these nozzles [15], therefore the differences observed between them in this study will not correspond to that phenomenon. The main characteristics of these injectors are summarized in the Table 1.

	Spray A	**Spray D**
Actual diameter [Do] (μm)	89.4	190.3
Nozzle K factor	1.5	1.5

Table 1. Characteristics of the injectors used in this study

In Table 2, the main characteristics of the tested fuels are presented. The fuel matrix includes reference and renewable fuels. The first group comprises standard Diesel as well as dodecane with a purity greater than 95% which is the standard fuel for ECN. Renewable fuels include Hydrotreated Vegetable Oil

(HVO), and two oxygenated fuels characterized by a general molecular structure: CH3–O–(CH2–O)n–CH3. The short name for this molecule is OMEn where n indicates the number of oxymethylene groups. One of them was the Dimethoxymethane, also known as Methylal (OME1) with 99.8% of purity; the other, here labelled as oxymethylene-dymethyl ether (OME_x) is a blend of several OME_n with the following mass ratios: 57.9% of OME_3, 28.87% of OME_4, 10.08% of OME_5 and 1.91% of OME_6.

Characteristics	**Diesel**	**Dodecane**	**HVO**	**OME_1**	**OME_x**
Density [kg/m^3] (T= 15 °C)	835.2	751.2	779.1	866.7	1057.1
Viscosity [mm^2/s] (T= 40 °C)	2.8	1.44	2.7	0.36	1.08
Cetane number [-]	54.18	74	75.5	28	68.6
Lubricity [µm]	386	563	316	747	320
Flash point [ºC]	-	83	70	<40	65
Lower heating value [MJ/kg]	39.79	44.2	43.90	19.25	19.21
Initial Boiling Point [ºC]	155.1	214	185.50	37.4	144.9
Final Boiling Point [ºC]	363.1	218	302	38	242.4
Average boing point [ºC]	259.1	216	243.75	37.7	193.65
Total contamination [mg/kg]	<24	-	6.0	<1	<1
Carbon content [% m/m]	85.3	84	85.7	48.4	44.2
Hydrogen Content [% m/m]	13.4	16	14.3	10.4	8.8
Oxygen content [% m/m]	0	0	0	42.1	45
$(A/F)_{st}$ at 15% of O_2	19.98	20.72	20.2	10.03	8.18

Table 2. Fuel properties.

2.3 Test matrix

Each fuel has been tested using the two injectors under the operating conditions depicted in Table 3. Starting from a baseline condition (900 K, 15% O_2 and 1500 bar injection pressure) different sweeps in temperature and injection pressure have been carried out. Ambient density inside the combustion chamber and oxygen mole fraction were kept constant along all the experimental conditions and equal to the reference value of 22.8 kg/m3 and 15%, respectively and consequently ambient pressure was adjusted for each temperature value.

Oxygen concentration (%)	**Density [kg/m3]**	**Temperature [K]**	**Injection Pressure [bar]**
15	22.8	800/**900**/1000	500/1000/**1500**

Table 3. Test matrix. The bold numbers represent the baseline operating condition.

The injection strategy was formed by a single injection pulse. The energizing time was 2 ms. A minimum of 20 injection cycles were recorded per case, to obtain statistically relevant results.

2.4 Diagnostic techniques

The optical techniques and experimental setup used in this work is exactly the same as detailed in [16]. It is sketched in Figure 1 and it will be only summarized here. In a first set of measurements, the high-speed schlieren imaging technique is used to capture the vapor penetration and Ignition Delay (ID), simultaneously to the recording of OH^* chemiluminescence with an intensified high-speed camera for the measurement of the flame Lift-off length (LOL). These two cameras (both Photron Fastacam SA-5) are labelled as 1 and 2 in Figure 1. For illumination in the schlieren imaging technique, a CW Xenon lamp was used with a BG18 filter, to generate a 150 mm diameter parallel illumination beam with a parabolic mirror. Another BG18 filter is used in front of the camera lens to reduce the effect of the sooting flame radiation on the schlieren images. For OH^* chemiluminescence imaging, the high-speed camera is equipped with a fast intensifier (Hamamatsu C10880), coupled to the camera with a 1:1 relay optics, and a UV lens. A 310 nm interference filter (10 nm FWHM) is used to filter out any other radiation from the flame. To allow the simultaneous operation of both techniques, a dichroic filter is used to reflect most of the UV radiation at 310nm whilst most of the visible radiation is transmitted to the schlieren camera.

Immediately after recording the schlieren and DBI images for every test case, a set of red LEDs (660 nm) and an engineered diffuser are set into the arrangement and aligned within few seconds by means of a translational stage (this motion is illustrated with a red arrow in Figure 1). The pulsation of these LEDs is synchronized with the frames of a Photron Fastcam SA-X2 camera (labelled as 3 in Figure 1), so that the extinction of light by the soot particles can be quantified with the DBI system, as described in [16]. All the image processing methods used follow the recommendations of the ECN and details on how the magnitudes for the analyses made here are derived from the images taken can be found in [16].

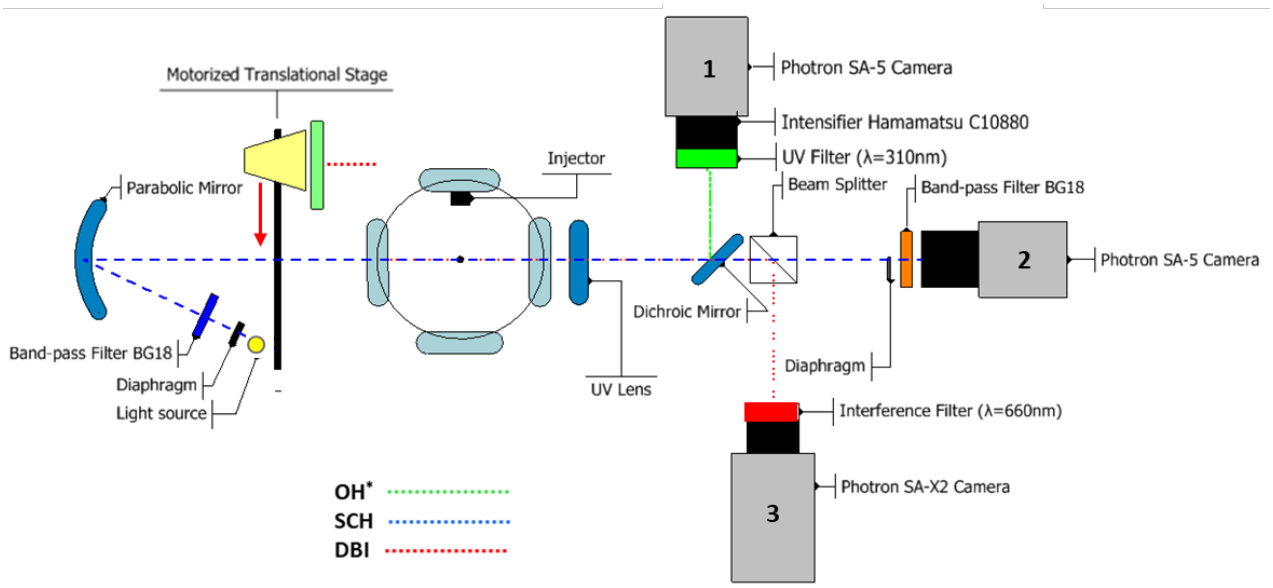

Figure 1. Optical configuration to measure the spray characteristics and combustion behavior for spray A and spray D and different alkanes and oxygenated fuels.

		Optical Technique	
Parameter	**Schlieren**	**OH***	**DBI**
Camera	Photron Fastcam SA5	Photron Fastcam SA5 + Hamamatsu C10880	Photron Fastcam SA-X2
Exposure time (µsec)	6.53	20 - 40	1
Filters	BG18	λ=310 nm (FWHM=10nm)	λ=660 nm (FWHM=10nm)
Resolution (pixel)	800x320	704x416	896x384
Frame rate (kfps)	25	25	12.5
Pixel/mm	6.9	5.43	6.85

Table 4. Configuration of each technique used in the optical set up

3 Results and Discussion

3.1 Spray tip penetration and liquid length

In Figure 2 the temporal evolution of vapor penetration, liquid length and lift-off length is shown, as well as the ignition delay obtained with both nozzles under the reference operating condition, namely 900 K, 15% of O_2 and 1500 bar of injection pressure. The shadow in each parameter represents its standard deviation. For the sake of simplifying, two fuels have been represented: HVO and OME_1. The red lines correspond to Spray D, and the black ones to Spray A. Hereafter, these nozzles will be

abbreviated as SA and SD. The trend for HVO is analogous to diesel and dodecane, while the trend for OME_1 is similar to OME_x except for the autoignition characteristics. The individual results for diesel, dodecane and OME_x can be found in Appendix A.

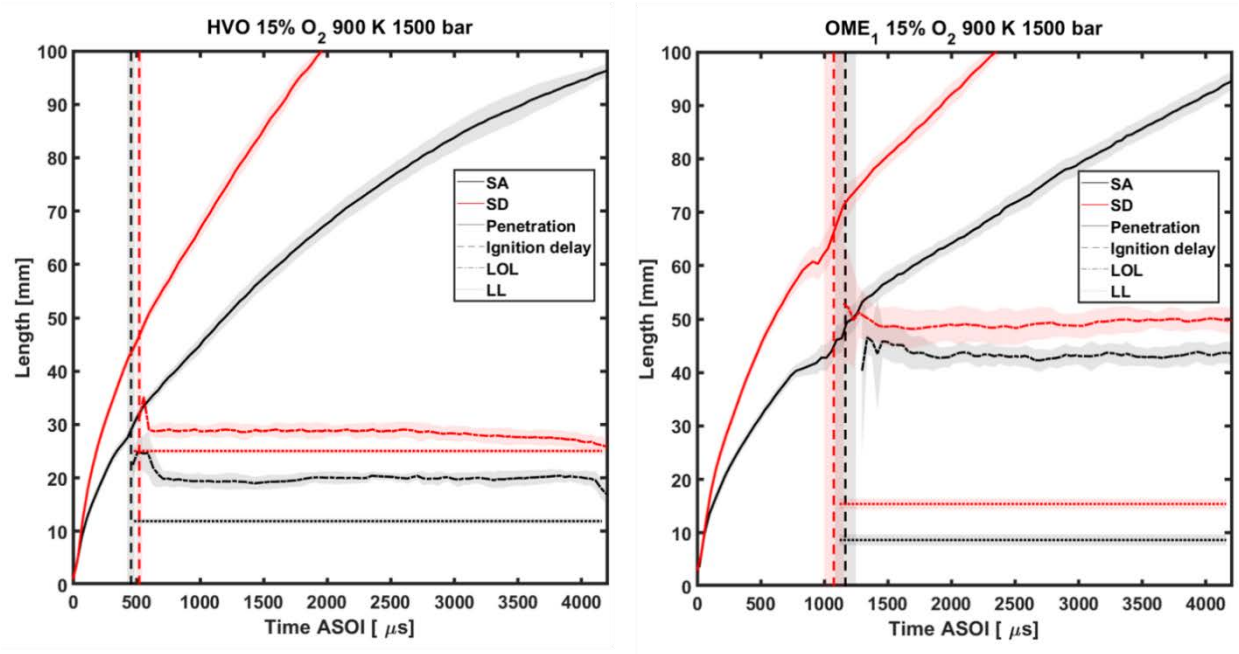

Figure 2. Comparison of the effect of nozzle diameter for HVO (left) and OME_1 (right) on the characteristic spray parameters.

For both fuels SD has a faster penetration than SA, as expected. The differences observed between injectors with respect to vapor penetration are the result of the momentum flux increment which is dependent on nozzle diameter. Only in the first instants, when the injector section is still controlled by the needle lift, both nozzles behave similar.

The stabilized Liquid Length (LL) as well as the Lift-off Length (LOL) are longer for SD. Additionally, Ignition Delay (ID) is also longer for this nozzle. As ambient conditions and fuel are exactly the same for both nozzles, these results suggest a slower mixing process for SD. That means also a slower vaporization process, which causes the ignition conditions to be achieved later.

When comparing both fuels, it is possible to see that changing the nozzle geometry does not have the same effect on each fuel. For HVO, the differences between the two nozzles are more noticeable than for OME_1. LL for HVO is 50% shorter for SA than for SD. However, for OME_1 only a 44% reduction is observed for the LL. When comparing autoignition, HVO shows a reduction in ID of 20% for SA with respect to SD. However, for OME_1 the ID trend is inverted, i.e. SA provides a 9% larger ID than SD does. The reason of this reverse trend will be analyzed in the following paragraphs. Finally, when focusing on the LOL, a reduction of 20% when comparing SA and SD has been measured for HVO while only a 12% difference is observed for OME_1.

The behavior reported in the previous paragraphs can be extended to the other fuels tested in this work and it can be found in Appendix A. On the one hand, diesel and HVO show a 50% reduction in LL, 20% in ID and 20% in LOL when comparing SA and SD. On the other hand, OME_x showed a similar behavior to OME_1. The main difference between the two oxygenated fuels is that the first one shows a trend similar as that of HVO in terms of ID when comparing SA and SD.

In Figure 3 the stabilized maximum liquid length for SD (LL_{SD}) versus SA (LL_{SA}) has been compared. Each fuel has been identified with a color, and the temperature with a symbol for easy understanding. The standard deviation has been represented with error bars. The dashed line has a slope equal to the ratio of actual diameters (Do) of both nozzles, as derived from Table 1. At constant operating conditions, this would be the theoretical relationship between the liquid length of both nozzles, according to scaling laws in [17,18]. In agreement with this scaling law, LL is longer for the SD. It is known that with bigger orifice diameters mixing slows down and atomization worsens [19]; as a consequence, the vaporization process slows down, too. The data corresponds to conditions with the longest separation between liquid and lift-off lengths (800 K and 900 K, 1500 bar injection pressure and 15% oxygen concentration) to ensure that the liquid length is not affected by combustion characteristics and then it can be considered as that of an inert spray. The variation of injection pressure has no effect on this parameter [20,21]. For that reason, just one pressure has been depicted.

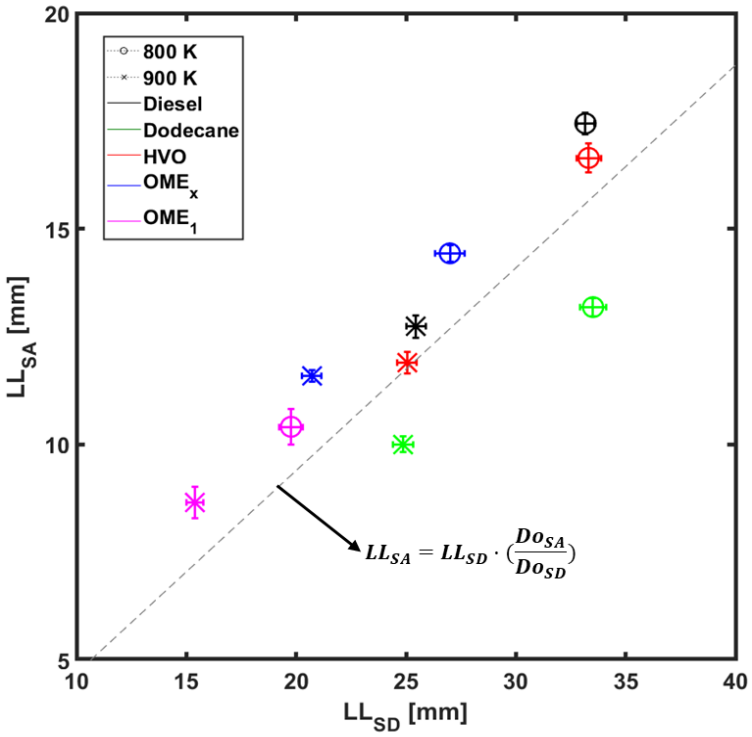

Figure 3. Liquid length comparison for Spray A and Spray D for diesel, dodecane, HVO, OME_x and OME_1. The operating conditions correspond to 800 K and 900 K at 15% of O_2 and 1500 bar of injection pressure.

Firstly, it can be observed that LL is closely linked to fuel composition as it has been reported previously [20]. Diesel, dodecane and HVO show similar values, while the OME_x and OME_1 have shorter LL. The fuels with lower distillation temperatures show shorter LL values as the vaporization process requires less energy to evaporate the fuel. This is coherent with the conclusions of Vera-Tudela [20] who stated that, after ambient temperature, the second greatest influence on the maximum liquid length is the enthalpy of vaporization. In the cases where this parameter is not available, the evaporation temperature or boiling point can be used instead [20,22]. The results in this study are in agreement with this statement, since the lowest average boiling point corresponds to OME_1 and then to OME_x, being HVO the fuel with higher boiling point of those represented. Regarding the differences between nozzle diameters, the LL is longer for the Spray D. It is known that with bigger orifice diameters the mixture mixing slows down and also worsens the atomization process[19] and as a consequence, the vaporization process worsens, too. The effect of nozzle diameter variation on the LL was lower for the oxygenated fuels because of the more similar volatility characteristics.

3.2 Combustion characteristics

Ignition delay (ID) results, are compared in Figure 4 for Spray A and Spray D. The operating conditions correspond to 800 K, 900 K and 1000 K at the two extreme injection pressures: 500 bar and 1500 bar.

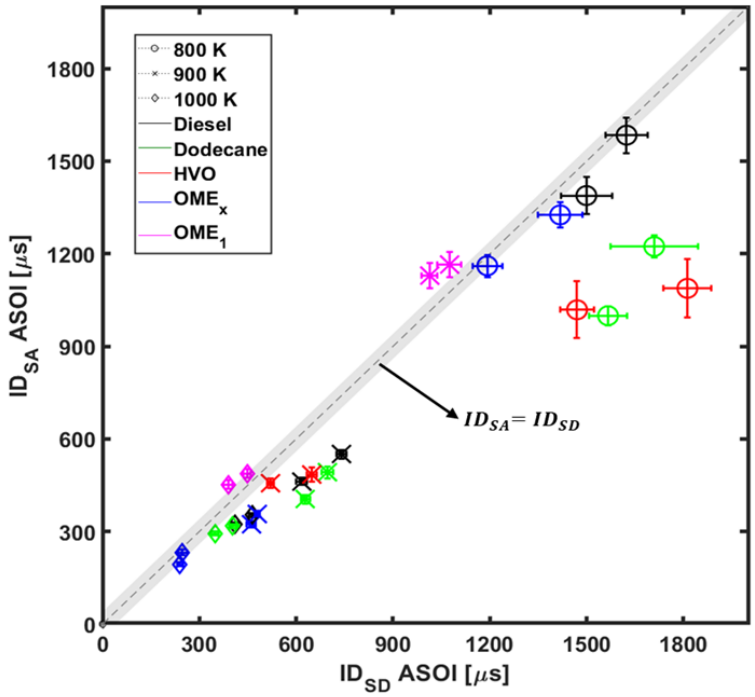

Figure 4 Ignition delay comparison between Spray A and Spray D for the five fuels tested. The data depicted corresponds to 800 K, 900 K and 1000 K at 500 and 1500 bar of injection pressure and 15% of O_2.

The different temperatures have been identified with symbols and the fuels with colors. Error bars correspond to the standard deviation. The gray shadow around the dashed line indicates a variation of ±40 μs, which was the high-speed camera shutter time used in this study, to represent the uncertainty related to the time resolution of the measurements. Spray D is shown to have around 20% longer ignition delay than Spray A for Diesel and HVO. For dodecane and OME_x this difference is around 30%. No special effect of fuel properties is observed. This trend has also been observed for dodecane in previous studies [15,23–25] and can be explained in terms of the slower mixing rate with the larger nozzle, which results in longer residence times needed to reach the mixture fraction values that are most favorable for ignition and hence a longer ignition timing.

However, the previous trend is not maintained for OME_1, where SA ignites later than SD. The larger nozzle provides an ID 9% shorter than the smaller one. Recent CFD computational results [26] have shown that for the nominal SA condition OME_1 combustion development occurs under highly lean conditions compared to dodecane. This is a consequence of the low reactivity of the fuel, coupled to the oxygen present in the fuel, which decreases the amount of stoichiometric air needed and hence result in a high degree of premixing at ignition sites. At the same time, concurrent homogeneous reactor calculations have also shown that from a purely chemical point of view the most reactive mixtures are close to stoichiometry, or even slightly rich. For this oxygenated fuel there seems to be a trade-off between the need to spend time in highly reactive mixtures for ignition to occur and the inherent fast mixing. In this context, the use of a larger nozzle diameter such as SD, which decreases mixing rate, means that more time can be spent on richer mixtures, which helps reduce ignition delay compared to the smaller nozzle. This is also consistent with results found in other studies [27] where it was indicated that for smaller nozzles diameter the ignition delay of oxygenated fuels is dominated by lean mixtures due to the fast air-fuel mixing. Figure 4 also shows that differences in ignition delay between nozzles for OME_1 reduce as ambient temperature increases, due to the higher reactivity, but results are never similar to those of the other fuels.

In Figure 5, Lift-off Length for Spray A and Spray D has been compared in different operating conditions. The different temperatures have been identified with symbols and the fuels with colors. The error bars represent the standard deviation. For all cases, LOL is higher when the Spray D is used. The dashed line represents the relation in which lift-off length is expected to vary with the nozzle diameter, as stablished by Siebers and Higgins [28]. They indicated that LOL is proportional to orifice diameter to the power of 0.34. The proportionality seems to fit the scatterplot on a global scale, but plenty of scattering can be observed, especially for low temperature (i.e. long LOL) cases. Error bars indicate that fluctuations become important for LOL values longer than 35 mm, due to the low reactivity.

In global terms, LOL follows the ID trend for diesel, dodecane, HVO and OME_x, which is in line with previous studies [29,30], meaning that longer ignition delays produce longer lift-off lengths. However,

it must be noted that for OME_1, LOL follows the same trend with respect to nozzle diameter as the other fuels, although this was not the case for ID, as discussed before. Current results show that, regardless nozzle diameter, presence of oxygen in the fuel molecule does not modify the relationship between ID and LOL, although other studies [31] have indicated that adding oxygen to the fuel reduces the ID and increases slightly the LOL.

To provide more insight into this behavior, the equivalence ratio at the lift-off length location ($\Phi_{cl,LOL}$) was calculated and depicted in Figure 6 for all operating conditions shown in Figure 5 according to Equation 1. The dotted line corresponds to the linear fit of the data and the constant *a* indicates its slope.

$$\Phi_{cl,LOL} = \frac{f_{cl,LOL}}{1 - f_{cl,LOL}} \cdot (A/F)_{st} \quad (1)$$

Where the term $f_{cl,LOL}$ refers to the fuel mixture fraction on the spray centerline at the lift-off length location. That term is determined using Equation 2:

$$f_{cl,LOL} = \frac{C \cdot Do \cdot \sqrt{\frac{\rho_f}{\rho_a}}}{LOL} \quad (2)$$

Where C is a constant with value equal to 7 [16], Do is the nozzle diameter and ρ_f and $\rho_a$represent the fuel and ambient density respectively.

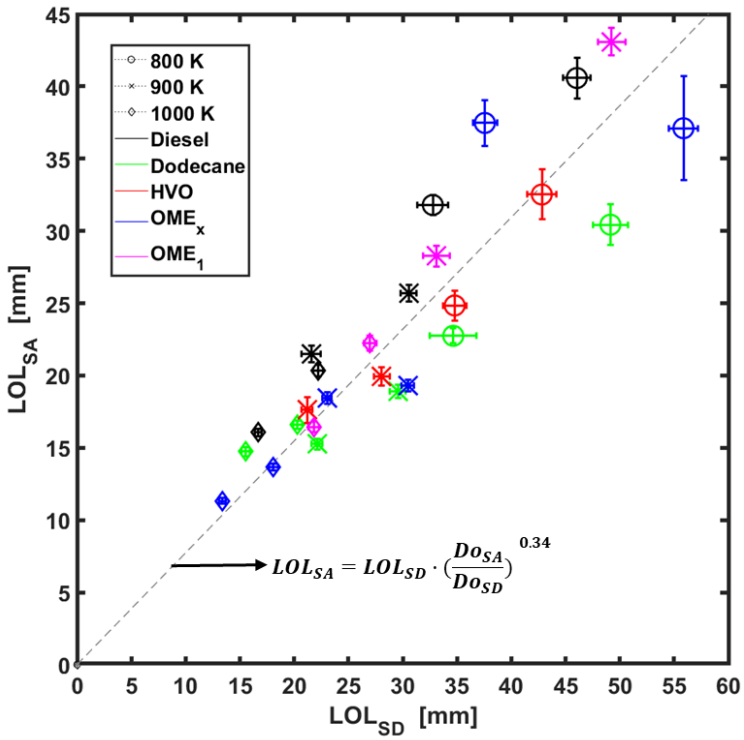

Figure 5 Lift-off length comparison between Spray A and Spray D for 800 K, 900 K and 1000 K and two injection pressures: 500 bar and 1500 bar. All cases at 15% of O_2.

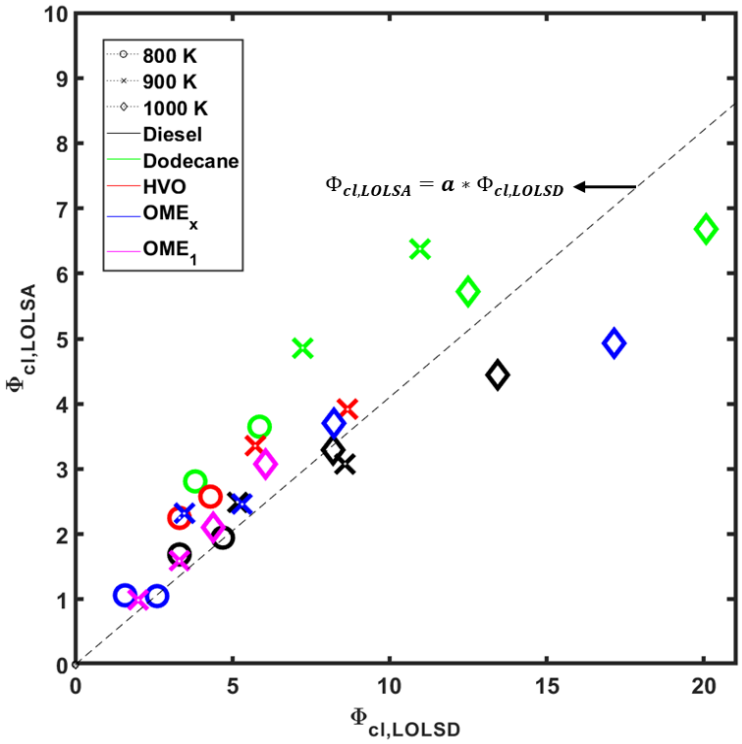

Figure 6. Comparison of the equivalence ratio at the lift-off ($\Phi_{cl,\,LOL}$) between Spray A and Spray D for each fuel and operating conditions shown in Figure 5

For all the fuels, SD nozzle provides richer $\Phi_{cl,LOL}$values than SA. As Equation 4 shows, in spite of the longer LOL values, the larger nozzle diameter results in richer $\Phi_{cl,LOL}$ values for SD than for SA. It must be noted that equivalence ratio value on the axis is an upper limit for the value that may be found at the lift-off location, as the actual flame is radially displaced from the axis, and hence even leaner values are expected. For oxygenated fuels, results confirm that even for the larger nozzle $\Phi_{cl,LOL}$ values can reach values close or below 2, which is in the range of non-sooting regimes.

To complement the previous analysis, Figure 7 shows overlaid schlieren (black) and OH^* (red) images for the nominal operating condition for all fuels and both nozzles for the quasi-steady phase of the reacting spray evolution (3015 µs ASOI). The first thing that can be observed is that the oxygenated fuel flames as defined from the OH^* signal for both nozzles are shorter and narrower than for the other fuels, consistently with the lower stoichiometric A/F ratio (Table 2). This is especially evident in SA images, where the observation window spans over the whole flame for all fuels due to the smaller nozzle diameter.

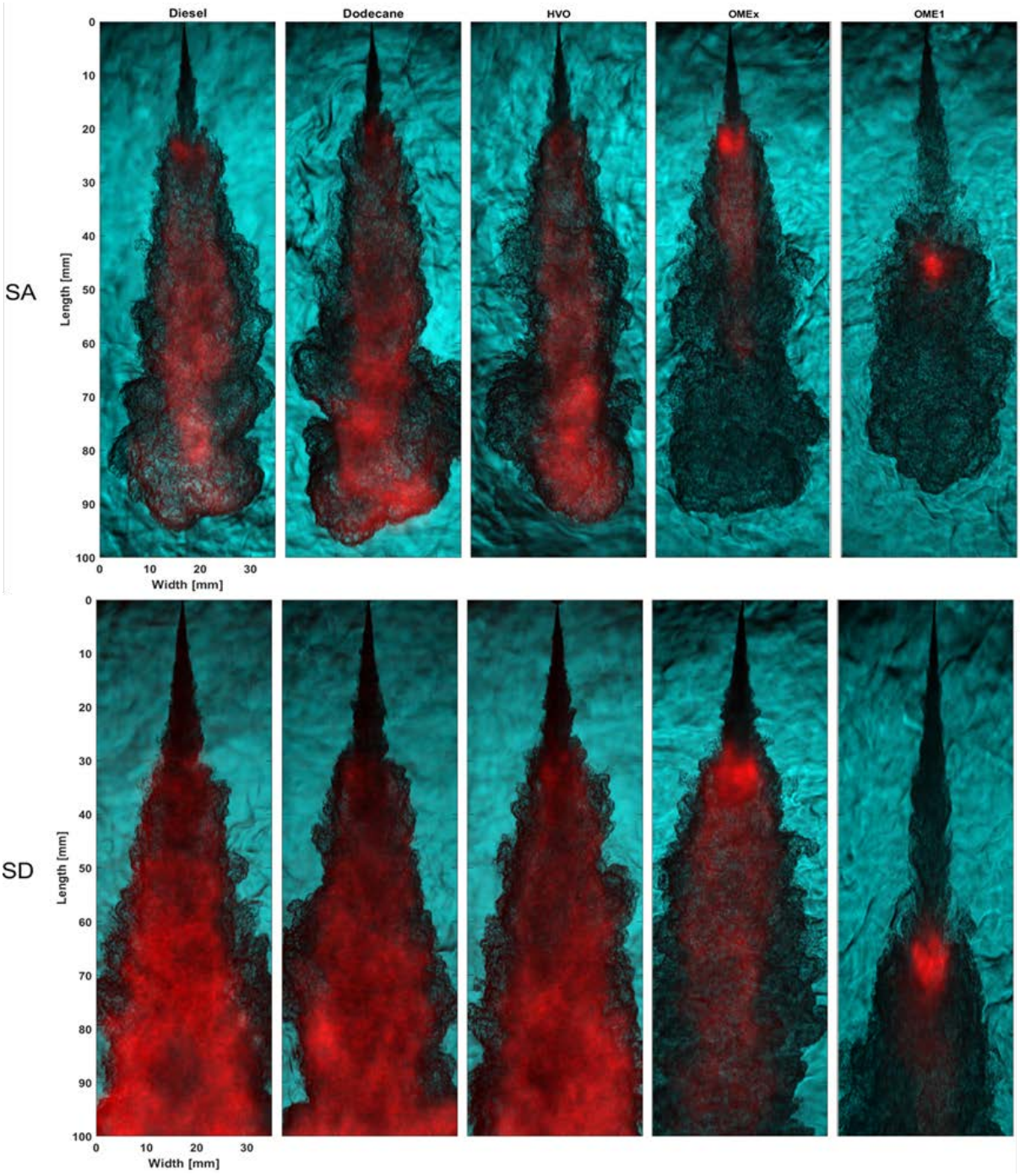

Figure 7. Overlaid images of schlieren and OH^* chemiluminescence images for different fuels and nozzle diameters for 900 K, 1500 bar of injection pressure and 15% of O_2 at 3015 µs.

OH^* images for diesel, dodecane and HVO show a typical cylindrical diffusion flame starting at the lift-off location [32] within a conical spray flow, as derived from the schlieren images. Moving from SA to SD, the spray flow increases in radius, the lift-off length location moves further away from the nozzle (as previously discussed) and there is a noticeable increase in OH^* signal intensity within the reaction zone compared to the smaller nozzle case. This intensity increases with axial distance to the orifice, which hints at an interference from soot broadband radiation. As results will show below, soot formation

is much larger in the larger nozzle, and most probably this creates a strong signal that overlaps with the OH^* one at 310 nm. All in all, fuel effects on flame radiation are not noticeable with these three fuels, and the transition from SA to SD is also similar for all of them.

For the oxygenated fuels, however, OH^* radiation distribution is pretty different. This is especially evident for OME_1 and the two nozzles, where the highest intensity all over the flame is observed at the lift-off location, with intensity dropping abruptly further downstream. This is consistent with results in [33] where flames with small nozzle diameter and oxygenated fuels were investigated. Under such conditions, lean equivalence ratio values were found at the flame base, in line with the results presented here (check $\Phi_{cl,LOL}$ in Figure 6). The whole combustion process is hence occurring at locally fuel-lean conditions. This result rules out the presence of a stoichiometric flame front, and hence some sort of lean-burn mixing-controlled combustion can be hypothesized in the same way as [33]. This reaction front location is pretty much the same for both nozzles, with the flame base moving from around 45 mm for SA to around 60 mm for SD. Other than that, there is no major difference between both nozzles.

For OME_x, some sort of in-between situation can be observed, with a LOL similar to the conventional fuels, and more luminosity downstream of this location. The equivalence ratio at the lift-off length is richer than for OME_1, and hence the possibility of a stabilized diffusion flame front around stoichiometric locations still exists.

3.2 Soot production

In Figure 8, the time-averaged (from 3 to 4 ms ASOI) KL distribution is shown for 900 K, 1500 bar of injection pressure and 15% O_2 for Spray D, which represents the quasi-steady combustion phase for all fuels. Maximum KL values are around 4 for Diesel, with slightly lower values for dodecane and HVO. However, not enough signal was found for OME_1 and OME_x , which confirms that these are non-sooting fuels as discussed in a previous work [16]. The molecular structure of these oxygenated fuels, without carbon-carbon bonds, avoid the soot formation [2,6] even under rich conditions as obtained for large nozzles as that SD (see Figure 6). In this figure it is also possible to see that the most sooting fuel is diesel, followed by dodecane and then HVO as the less sooting fuel of these three. This result is in agreement with results presented in [31] for different fuels blends, in which the higher KL values were for those blends with aromatic compounds, and the lower KL values were for blends with oxygenated fuels.

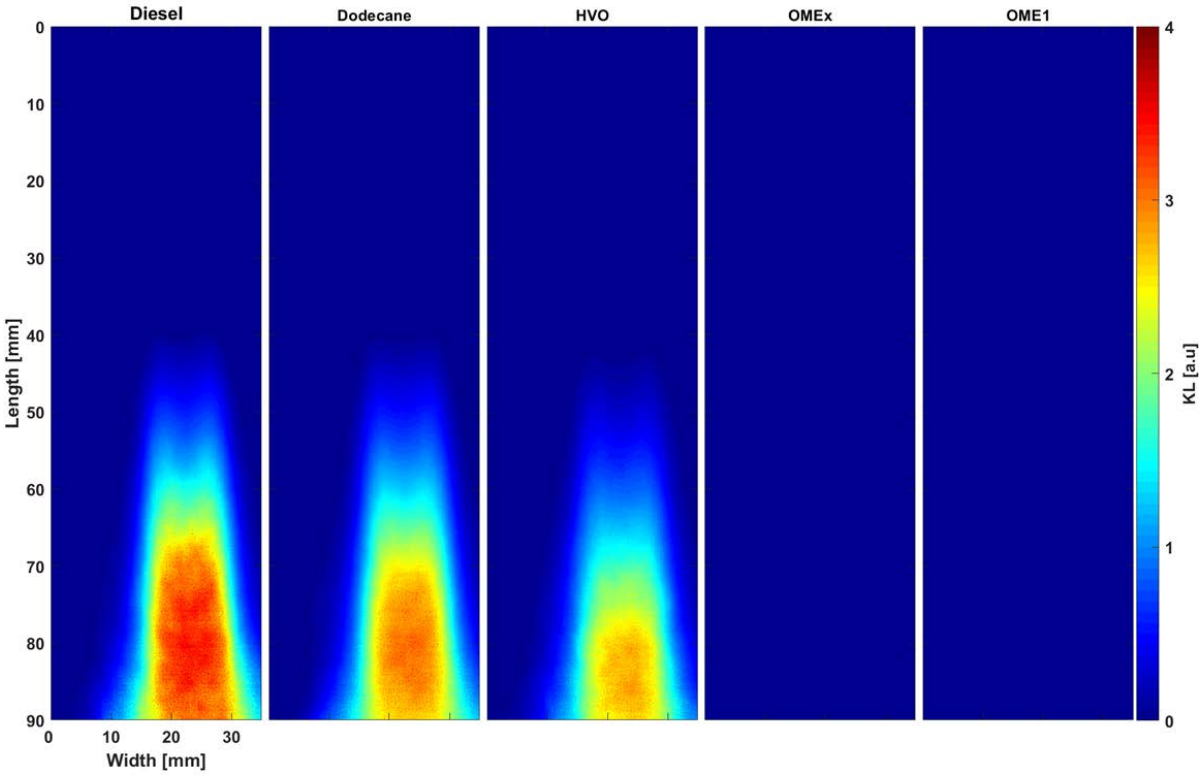

Figure 8. Average soot KL values for spray D during the quasi-steady phase of the flame, between 3 ms and 4 ms. The operating conditions are 900 K, 1500 bar of injection pressure and 15% of O_2

Figure 9 depicts the evolution of accumulated soot mass for diesel, dodecane and HVO at 900 K, 500 bar of injection pressure and 15% of O_2 for SA (solid lines) and SD (dotted lines). The shadows correspond to the confidence interval of the average at 95%. The total soot mass (s_{mass}) has been obtained transforming the value of the KL parameter, measured with DBI, to soot mass through the Equation 3.

$$s_{mass} = \frac{\sum KL \cdot \rho_{soot} \cdot \lambda}{k_e \cdot r^2} \qquad (3)$$

Where, ∑KL indicates the sum of KL values of all pixels at each recorded instant. The ρsoot corresponds to the soot density defined as 1.8 g/cm3 [34], λ is the wavelength of the light source used (660 nm in the current work), r is the pixel to mm ratio (6.85 px/mm) and k_e is the dimensionless soot extinction coefficient equal to 7.27, determined in this study through the ratio of soot scattering and absorption cross-sections which is used in small particle Mie theory

Fuel trends are consistent with those obtained in Figure 8, namely soot formation with diesel is higher than dodecane and HVO. With SD, the measured maximum soot value increases six to ten times with respect to the maximum obtained with SA. While the smaller SA nozzle remains within the field of view, Figure 8 shows that this is not the case for SD, and hence the total soot amount produced by this

nozzle cannot be measured. Therefore, the observed quantitative relationship between both nozzles is only an indication, the total soot formation in SD cases will be larger.

As previously discussed, although SD provides longer LOL for all the fuels, the corresponding $\Phi_{cl,LOL}$ is also higher due to the slower mixing rate. Thus, the combustion of richer mixtures with this nozzle leads high soot formation. Besides this richer mixture at the flame base, bigger orifice diameter promotes longer local residence time of fuel. This allows a greater formation of soot precursor species [19] and hence more soot production for the larger nozzles. This argument is in agreement with other authors who previously stated that the soot scales with the in-flame residence time [35].

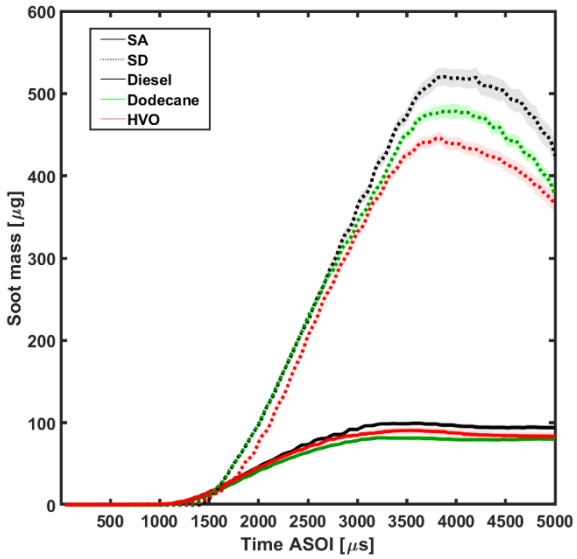

Figure 9 Comparison of accumulated soot mass production evolution of Spray A and Spray D. The operating conditions are 900 K, 500 bar and 15% of O_2.

4 Conclusions

The main spray parameters and combustion characteristics of five fuels, with different physical and chemical properties, have been analyzed in this study for two nozzles, namely Spray A (SA) and Spray D (SD) of the ECN, with orifice actual diameter of 89.4 µm and 190.3 µm respectively. The fuels were diesel, dodecane, HVO, OME_1 and OME_x. All experiments were carried out in a High Pressure and High Temperature facility. The baseline operating condition and a sweep of ambient pressure and temperature as well as injection pressure was performed following ECN guidelines. The main conclusions of this study are summarized below.

- Changing the nozzle diameter produces the same effect over combustion development for all fuels, but not with the same intensity. The differences in terms of molecular structure have shown a big influence in this regard. In the case of oxygenated fuels, the effect of changing the nozzle is not as significant as it is for the diesel, dodecane and HVO in terms of ignition and combustion development.

- For all cases, SD causes a faster penetration than SA. This can be explained due to the different momentum flux at the nozzle since SD has bigger orifice diameter than SA. A similar conclusion can be extracted regarding liquid length. The five fuels show a similar behavior when comparing SD with SA. The former one atomizes the fuel worst, which hinders fuel evaporation.
- Ignition delay for SD is, in general, higher than for SA. SD causes longer fuel residence times and, therefore, the slower mixing process affects the ignition process. However, for OME_1, the behavior is the opposite. At baseline operating condition, ID for SD was 9% smaller than for SA as a result of the low mixing rate with the SD, meaning that more time can be spent on richer mixture, which helps reduce ignition delay compared to the Spray A.
- Lift-off length follows a similar trend as ID for all fuels except OME_1. In this case, the lift-off for SD is longer than for SA as it was with the other fuels. The equivalence ratio at LOL was calculated for all the fuels and, in the case of OME_1, for the baseline operating condition, it was less or equal to 1 when SA was used. This is related with its molecular composition and indicates that the ignition process could be jeopardized by a fuel overmixture. In fact, the low equivalence ratio at LOL of this fuel for both nozzles suggest that the combustion process for SA could be closer to a premixed combustion than to a diffusive one, and in a sort of transition for SD.
- In terms of soot production, for the operating condition of 900 K, 500 bar and 15% of O_2 the dodecane with the Spray D produces eight times more soot than Spray A. In the case of diesel and HVO, the soot production was six and eleven times higher. That was a result of slower mixing process when bigger orifice diameter was used. The oxygenated fuels OME_1 and OME_x do not produce soot with any of the nozzles. Furthermore, the equivalence ratio at LOL is the lower, which would guarantee a minimum or null soot formation in case it existed. However, the non-soot formation of oxygenated fuels is also achieved thanks to molecular composition, which does not contain C-C bonds.

Acknowledgements

The authors acknowledge that this research work has been partly funded by the European Union's Horizon 2020 Programme, grant agreement n° 828947, and from the Mexican Department of Energy, CONACYT-SENER Hidrocarburos grant agreement n° B-S-69926 and by Universitat Politècnica de València through the Programa de Ayudas de Investigación y Desarrollo (PAID-01-18). Part of the equipment used in this work was funded by FEDER and GVA through contract IDIFEDER/2018/037.

Appendix A: Effect of nozzle diameter for diesel, dodecane and OME_x on the characteristic spray parameters.

In Figure 10, the main spray parameters for diesel, dodecane and OME_x have been represented. The operating condition correspond to the baseline (900K 1500 bar and 15% of O_2). These graphs allow

quantifying the effect of changing nozzle diameter on the main spray characteristics for diesel, dodecane and OME_x. This information is complementary to that presented in Figure 2.

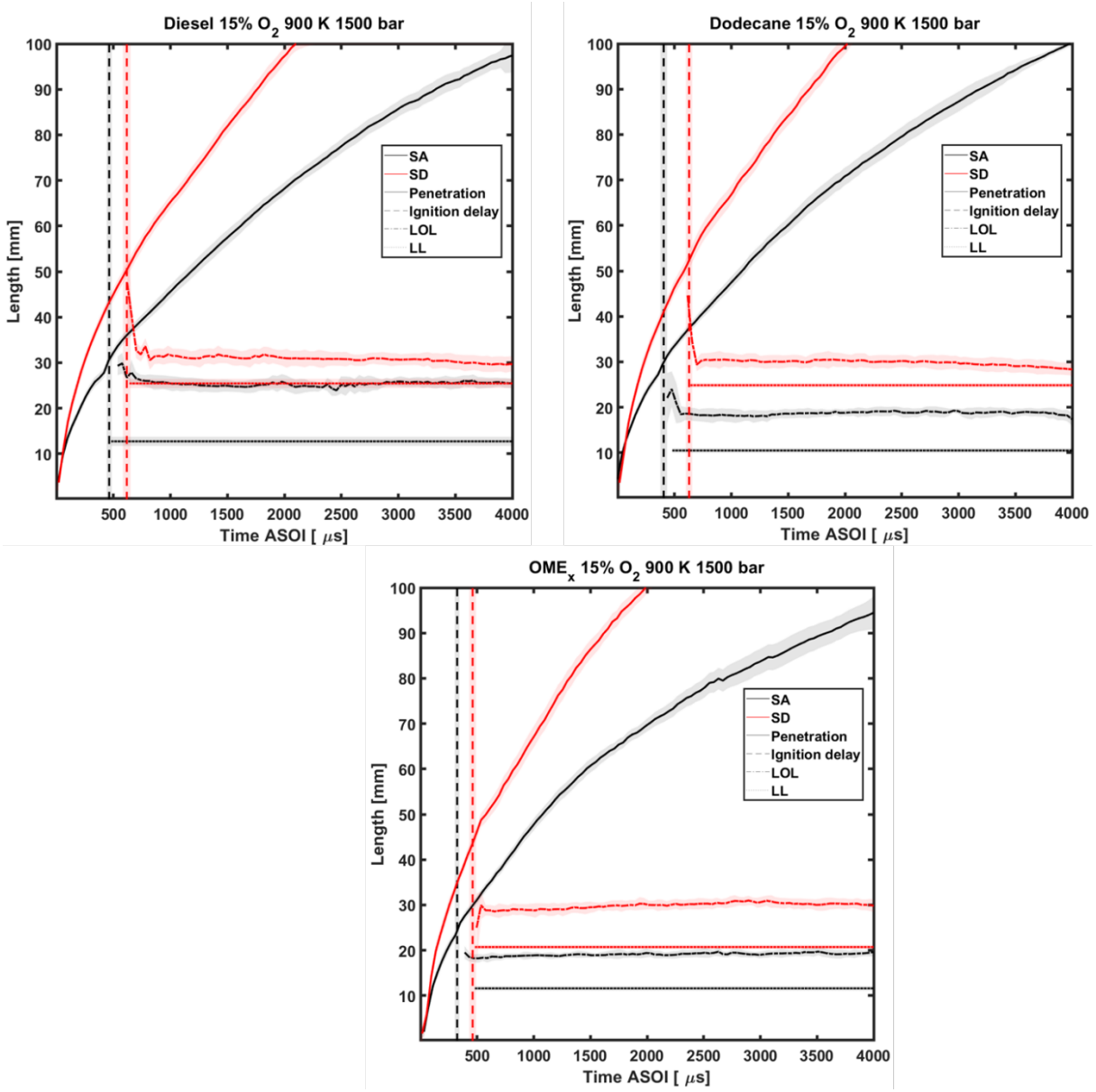

Figure 10. Comparison of the effect of nozzle diameter for diesel (top left), dodecane (top right) and OME_1 (bottom center) on the characteristic spray parameters for the baseline condition. The shadow in each parameter represents the standard deviation.

References

[1] Reitz RD, Ogawa, H, Payri, R. IJER Editorial: The Future of the Internal Combustion Engine. International Journal of Engine Research 2020;21:3–10. https://doi.org/10.1177/1468087419877990.

[2] Svensson KI, Richards MJ, Mackrory AJ, Tree DR. Fuel Composition and Molecular Structure Effects on Soot Formation in Direct-Injection Flames Under Diesel Engine Conditions, SAE Technical Paper 2005-01-0381; 2005. https://doi.org/10.4271/2005-01-0381.
[3] Dimitriadis A, Seljak T, Vihar R, Žvar Baškovič U, Dimaratos A, Bezergianni S, et al. Improving PM-NOx trade-off with paraffinic fuels: A study towards diesel engine optimization with HVO. Fuel 2020;265:116921. https://doi.org/10.1016/j.fuel.2019.116921.
[4] Burger J, Siegert M, Ströfer E, Hasse H. Poly(oxymethylene) dimethyl ethers as components of tailored diesel fuel: Properties, synthesis and purification concepts. Fuel 2010;89:3315–9. https://doi.org/10.1016/j.fuel.2010.05.014.
[5] Schmitz N, Burger J, Ströfer E, Hasse H. From methanol to the oxygenated diesel fuel poly (oxymethylene) dimethyl ether: An assessment of the production costs. Fuel 2016;185:67–72. https://doi.org/10.1016/j.fuel.2016.07.085.
[6] Omari A, Heuser B, Pischinger S. Potential of oxymethylenether-diesel blends for ultra-low emission engines. Fuel 2017;209:232–7. https://doi.org/10.1016/j.fuel.2017.07.107.
[7] Benajes J, García A, Monsalve-Serrano J, Martínez-Boggio S. Potential of using OMEx as substitute of diesel in the dual-fuel combustion mode to reduce the global CO2 emissions. Transportation Engineering 2020;1:100001. https://doi.org/10.1016/j.treng.2020.01.001.
[8] Njere D, Emekwuru N. Fuel spray vapour distribution correlations for a high pressure diesel fuel spray cases for different injector nozzle geometries. Proceedings ILASS–Europe 2017. 28th Conference on Liquid Atomization and Spray Systems, Universitat Politècnica de València; 2017. https://doi.org/10.4995/ILASS2017.2017.4951.
[9] Som S, Aggarwal SK, El-Hannouny EM, Longman DE. Investigation of Nozzle Flow and Cavitation Characteristics in a Diesel Injector. J Eng Gas Turbines Power. April 2010;132(4):042802. https://doi.org/10.1115/1.3203146.
[10] Payri R, Garcia J, Salvador F, Gimeno J. Using spray momentum flux measurements to understand the influence of diesel nozzle geometry on spray characteristics. Fuel 2005;84:551–61. https://doi.org/10.1016/j.fuel.2004.10.009.
[11] Blessing M, König G, Krüger C, Michels U, Schwarz V. Analysis of Flow and Cavitation Phenomena in Diesel Injection Nozzles and Its Effects on Spray and Mixture Formation, SAE Technical Paper 2003-01-1358; 2003. https://doi.org/10.4271/2003-01-1358.
[12] Payri F, Margot X, Patouna S, Ravet F, Funk M. A CFD Study of the Effect of the Needle Movement on the Cavitation Pattern of Diesel Injectors SAE Technical Paper 2009-24-0025, 2009, https://doi.org/10.4271/2009-24-0025.
[13] Engine Combustion Network | Engine Combustion Network Website (July 2021). https://ecn.sandia.gov/.
[14] Payri R, Gimeno J, Bardi M, Plazas AH. Study liquid length penetration results obtained with a direct acting piezo electric injector. Applied Energy 2013;106:152–62. https://doi.org/10.1016/j.apenergy.2013.01.027.
[15] Pastor JV, Garcia-Oliver JM, Garcia A, Morales López A. An Experimental Investigation on Spray Mixing and Combustion Characteristics for Spray C/D Nozzles in a Constant Pressure Vessel, SAE Technical Paper 2018-01-1783; 2018. https://doi.org/10.4271/2018-01-1783.
[16] Pastor JV, García-Oliver JM, Micó C, García-Carrero AA, Gómez A. Experimental Study of the Effect of Hydrotreated Vegetable Oil and Oxymethylene Ethers on Main Spray and Combustion Characteristics under Engine Combustion Network Spray A Conditions. Applied Sciences 2020;10:5460. https://doi.org/10.3390/app10165460.
[17] Pickett LM, Kook S, Williams TC. Transient Liquid Penetration of Early-Injection Diesel Sprays. SAE Int J Engines2 (1):785-804, 2009. https://doi.org/10.4271/2009-01-0839.
[18] Siebers DL. Scaling Liquid-Phase Fuel Penetration in Diesel Sprays Based on Mixing-Limited Vaporization, SAE Technical Paper; 1999. https://doi.org/10.4271/1999-01-0528.
[19] Pachano, L. CFD modeling of combustion and soot production in diesel sprays. PhD thesis. Universitat Politècnica de València, 2020.
[20] Vera-Tudela Fajardo WM. An experimental study of the effects of fuel properties on diesel spray processes using blends of single-component fuels. PhD thesis. Universitat Politècnica de València, 2015.

[21] Pastor J, Garcia-Oliver JM, Garcia A, Nareddy VR. Characterization of Spray Evaporation and Mixing Using Blends of Commercial Gasoline and Diesel Fuels in Engine-Like Conditions, SAE Technical Paper 2017-01-0843; 2017. https://doi.org/doi:10.4271/2017-01-0843.
[22] Kook S, Pickett LM. Liquid length and vapor penetration of conventional, Fischer–Tropsch, coal-derived, and surrogate fuel sprays at high-temperature and high-pressure ambient conditions. Fuel 2012;93:539–48. https://doi.org/10.1016/j.fuel.2011.10.004.
[23] Desantes JM, Garcia-Oliver JM, Novella R, Pachano L. A numerical study of the effect of nozzle diameter on diesel combustion ignition and flame stabilization. International Journal of Engine Research 2020;21:101–21. https://doi.org/10.1177/1468087419864203.
[24] Maes N, Skeen SA, Bardi M, Fitzgerald RP, Malbec L-M, Bruneaux G, et al. Spray penetration, combustion, and soot formation characteristics of the ECN Spray C and Spray D injectors in multiple combustion facilities. Applied Thermal Engineering 2020;172:115136. https://doi.org/10.1016/j.applthermaleng.2020.115136.
[25] Pérez-Sánchez EJ, Garcia-Oliver JM, Novella R, Pastor JM. Understanding the diesel-like spray characteristics applying a flamelet-based combustion model and detailed large eddy simulations. International Journal of Engine Research 2020;21:134–50. https://doi.org/10.1177/1468087419864469.
[26] Benajes J, Garcia-Oliver JM, Pastor JM, De-Leon-Ceriani D. A computational study on OME1 spray combustion under ECN Spray A conditions, Zhenjiang, China: ILASS-Asia; 2020.
[27] Zubel M, Ottenwälder T, Heuser B, Pischinger S. Combustion system optimization for dimethyl ether using a genetic algorithm. International Journal of Engine Research 2021;22:22–38. https://doi.org/10.1177/1468087419851577.
[28] Siebers D, Higgins B. Flame Lift-Off on Direct-Injection Diesel Sprays Under Quiescent Conditions, SAE Technical Paper 2001-01-0530; 2001. https://doi.org/10.4271/2001-01-0530.
[29] Benajes J, Payri R, Bardi M, Martí-Aldaraví P. Experimental characterization of diesel ignition and lift-off length using a single-hole ECN injector. Applied Thermal Engineering 2013;58:554–63. https://doi.org/10.1016/j.applthermaleng.2013.04.044.
[30] Pickett LM, Siebers DL, Idicheria CA. Relationship Between Ignition Processes and the Lift-Off Length of Diesel Fuel Jets, SAE Technical Paper 2005-01-384; 2005. https://doi.org/10.4271/2005-01-3843.
[31] Manin J, Skeen S, Pickett L, Kurtz E, Anderson JE. Effects of Oxygenated Fuels on Combustion and Soot Formation/Oxidation Processes. SAE Int J. Fuels Lubr. 7(3):704-717, 2014. https://doi.org/10.4271/2014-01-2657.
[32] Dec JE, Coy EB. OH Radical Imaging in a DI Diesel Engine and the Structure of the Early Diffusion Flame, SAE Technical Paper 960831; 1996. https://doi.org/10.4271/960831.
[33] Pickett LM, Siebers DL. Non-Sooting, Low Flame Temperature Mixing-Controlled DI Diesel Combustion, SAE Technical Paper 2004-01-1399; 2004. https://doi.org/10.4271/2004-01-1399.
[34] Choi MY, Mulholland GW, Hamins A, Kashiwagi T. Comparisons of the soot volume fraction using gravimetric and light extinction techniques. Combustion and Flame 1995;102:161–9. https://doi.org/10.1016/0010-2180(94)00282-W.
[35] Foo KK, Sun Z, Medwell PR, Alwahabi ZT, Nathan GJ, Dally BB. Influence of nozzle diameter on soot evolution in acoustically forced laminar non-premixed flames. Combustion and Flame 2018;194:376–86. https://doi.org/10.1016/j.combustflame.2018.05.026.

Abbreviations

$(A/F)_{st}$: Stoichiometric air–fuel ratio

ASOI: After Start of Injection

C: constant with value equal to 7

CI: Compression Ignition

ECN: Engine Combustion Network

Do: Actual Nozzle Diameter

F: Focal length

FWHM: Full Width at Half Maximum

HVO: Hydrotreated Vegetable Oil

ICCD: Intensified Charge –Coupled Device

ID: Ignition Delay

KL: Optical Thickness

LED: Light-Emitting Diode

LL: Liquid Length

LOL: Lift-off Length

NO_x: Nitrogen Oxides

OH^{*}: Excited state of hydroxyl radical

OME_1: simplest molecular structure of oxymethylene ethers $CH_3–O–(CH_2–O)_n–CH_3$ n=1

OME_x: A blend of oxymethylene ethers

PM: Particle Matter

SA: Spray A

SD: Spray D

SOI: Start of Injection

$f_{cl,LOL}$: Fuel mixture fraction on the spray centerline

$\Phi_{cl,LOL}$: Equivalence ratio at the lift-off length location

s_{mass}: soot mas

KL: Integral value of the soot extinction coefficient along the light path

λ: Wavelength

k_e: Dimensionless soot extinction coefficient

r: Pixel-mm ratio (px/mm)